

# Spermidine-Induced Attraction of Like-Charged Surfaces Is Correlated with the pH-Dependent Spermidine Charge: Force Spectroscopy Characterization

Jan Gimsa,<sup>\*,†</sup> Philipp Wysotzki,<sup>†</sup> Šarka Perutkova,<sup>‡</sup> Thomas Weihe,<sup>§</sup> Patrick Elter,<sup>||</sup> Piotr Marszałek,<sup>⊥</sup> Veronika Kralj-Iglič,<sup>#</sup> Torsten Müller,<sup>¶</sup> and Aleš Iglič<sup>\*,‡</sup>

<sup>†</sup>Department of Biophysics, Faculty of Natural Sciences, University of Rostock, 18057 Rostock, Germany

<sup>‡</sup>Laboratory of Biophysics, Faculty of Electrical Engineering, University of Ljubljana, 1000 Ljubljana, Slovenia

<sup>§</sup>Leibniz Institute for Plasma Science and Technology, 17489 Greifswald, Germany

<sup>||</sup>Department of Life Science Engineering, University of Applied Sciences Mittelhessen, 35390 Gießen, Germany

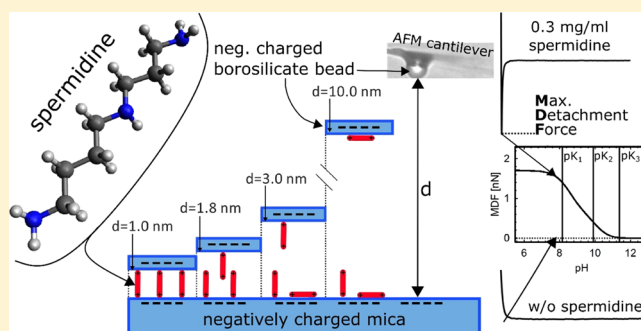
<sup>⊥</sup>Department of Mechanical Engineering and Material Science, and Center for Biologically Inspired Materials and Material Systems, Duke University, Durham, North Carolina 27708, United States

<sup>#</sup>Laboratory of Clinical Biophysics, Faculty of Health Sciences, University of Ljubljana, 1000 Ljubljana, Slovenia

<sup>¶</sup>R&D Department, JPK Instruments AG, 12099 Berlin, Germany

## Supporting Information

**ABSTRACT:** The ubiquitous molecule spermidine is known for its pivotal roles in the contact mediation, fusion, and reorganization of biological membranes and DNA. In our model system, borosilicate beads were attached to atomic force microscopy cantilevers and used to probe mica surfaces to study the details of the spermidine-induced attractions. The negative surface charges of both materials were largely constant over the measured pH range of pH 7.8 to 12. The repulsion observed between the surfaces turned into attraction after the addition of spermidine. The attractive force was correlated with the degree of spermidine protonation, which changed from +3 to +1 over the measured pH range. The force was maximal at pH 7.8. To explain the observed pH and spermidine concentration dependence, two different theoretical approaches were used: a chemical model of the charge equilibrium of spermidine and Monte-Carlo simulations of the orientation of the rodlike spermidine molecules in the gap between the borosilicate and mica surfaces. Monte-Carlo simulations of the orientational ordering of the rodlike spermidine molecules suggested the induction of attractive interactions between the surfaces if the gap was bridged by the molecules. For larger gaps, the orientational distribution function of the spermidine molecules predicted a considerable degree of parallel attachment of the molecules to the surfaces, resulting in reduced effective surface charge densities of both surfaces, which reduced their electrostatic repulsion.



## INTRODUCTION

As early as 1677, van Leeuwenhoek described crystals in human spermatozoa. These crystals contain an amazingly high concentration of 3.3 mg/mL of spermine, which is synthesized from spermidine.<sup>1</sup> Spermidine is a rodlike polycation with three nitrogen atoms in a carbon chain (Figure 1). Depending on the pH, it may carry a maximum of three positive charges located at the two terminal amino groups and the central imine group. The investigation of their pH-dependent protonation by <sup>13</sup>C NMR spectroscopy revealed pK<sub>a</sub> values of pK<sub>1</sub> = 8.25 ± 0.09, pK<sub>2</sub> = 9.71 ± 0.12, and pK<sub>3</sub> = 10.90 ± 0.21.<sup>2</sup>

Spermidine has a wide variety of physiological functions, for example, in inflammation reduction, lipid metabolism, regulation of cell growth, proliferation, apoptosis, and so forth.<sup>3</sup> The presence of spermidine or spermine is required for the

stabilization of double-stranded RNA during replication.<sup>4</sup> Spermidine has been shown to induce autophagy in a wide variety of higher organisms and even in worms or yeast.<sup>5</sup> Positive effects on the aging process have also been discussed.<sup>3</sup>

Spermidine, which is triprotonated under physiological conditions, plays a role in specific receptor–ligand binding processes and may mediate the unspecific interaction of negatively like-charged surfaces, for example, of cells, vesicles, and macromolecules in many biological processes.<sup>6–9</sup> The agglutination of giant unilamellar vesicles (GUVs) has been used as a model system of mutually repulsive negatively like-

Received: December 13, 2017

Revised: January 18, 2018

Published: January 30, 2018

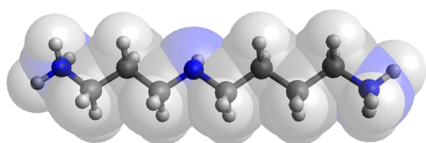


**Figure 1.** Ball-and-stick representation of a diprotonated spermidine molecule with carbon (black), hydrogen (white), and nitrogen (blue) atoms. In the minimal energy (vacuum) conformation, the distance between the two terminal amino groups is approx. 11 Å (computed with Avogadro, “an open-source molecular builder and visualization tool”, version 1.1.1).

charged surfaces.<sup>6,10</sup> Spermidine is also important for contact control in semibiological systems, for example, in the process of implant integration.<sup>11–15</sup>

The DLVO theory provides a straightforward approach to explaining these effects by considering the superposition of electrostatic and van der Waals forces.<sup>16,17</sup> In the classical approach, electrostatic double-layer repulsion, which dominates at long distances may be overcome by van der Waals attraction at short distances. This approach correctly describes many phenomena in biological systems, for example, unspecific interactions, which are important in the initial processes of aggregation and adhesion.<sup>18</sup>

The DLVO theory has been refined by ion-correlation and ion-condensation effects.<sup>17</sup> Ion correlation has experimentally been observed with polyvalent macroions by Kirkwood and Shumaker before it was studied with Monte-Carlo simulations.<sup>19–21</sup> Oosawa predicted the condensation of large ions after he investigated charge fluctuations in the counterion cloud of polyions.<sup>22</sup> These fluctuations generate attractive forces between the induced dipole of the ion clouds of adjacent electric double layers.

To investigate how the degree of spermidine protonation modulates the attractive forces between negatively like-charged surfaces, we used freshly cleaved sheets of muscovite mica and borosilicate beads as a model system. The charge of these surfaces is known to be largely pH-independent above pH 7.0.<sup>23</sup> We attached commercial borosilicate beads to atomic force microscopy (AFM) cantilevers to investigate the spermidine concentration and pH dependence of the interaction forces of the negatively like-charged surfaces.

Mica ( $\text{KAl}_2[\text{Si}_3\text{AlO}_{10}](\text{OH})_2$ ) is a 2:1 clay mineral, that is, one elementary sheet contains two layers of  $[\text{Si}_3\text{AlO}_{10}]^{5-}$  that are zipped together by a layer of partly hydroxylated  $\text{Al}^{3+}$  ions. Potassium ions compensate for the resulting net charge and form linkages between the single sheets. The chemical weakness of this coupling results in the good cleavability of mica, yielding nearly ideal, atomically flat thin sheets.<sup>24,25</sup>

Borosilicate beads are known for their pH-independent negative zeta potential.<sup>23,26</sup> This potential results from the isoelectric point of borosilicate being below pH 3.<sup>27</sup> Chemically, the pH-independent zeta potential is based on the hydroxyl groups of silicon and boron,<sup>28</sup> which provide the major charge contributions.<sup>29</sup>

## EXPERIMENTAL SECTION

**AFM Setup.** The force measurements were carried out with a NanoWizard II AFM (JPK Instruments, Berlin, Germany) mounted on an inverted fluorescence microscope (Axio Observer A1, Carl Zeiss, Jena, Germany). The AFM head was equipped with a linearized

piezoelectric scanner with a 15 μm z-range and an infrared laser-lever system. The measurements were conducted in Petri dishes (diameter 40 mm; TPP, Trasadingen, Switzerland), which were placed in a thermostated Petri dish heater (JPK Instruments, Berlin, Germany). The measurement parameters were determined using JPK’s SPM Control Software v. 3.

**Solutions.** Crystalline spermidine trihydrochloride (Sigma-Aldrich, Taufkirchen, Germany) was dissolved in deionized water to a concentration of 1 mg/mL. This solution had a pH of  $5.90 \pm 0.05$ . The desired pH values of 7.0, 7.8, 9.0, 10.5, or 12 were achieved by the addition of sodium hydroxide (Carl Roth, Karlsruhe, Germany) with stirring and pH monitoring. To prepare the spermidine dilution series, the pH-adjusted spermidine stock solution was diluted with titrated deionized water. At each pH value, the AFM measurements were started in deionized water without spermidine and then continued in solutions of spermidine at different concentrations in an ascending order over a range of 0.01 to 0.1 mg/mL. At each pH value, 1000 force–distance curves were recorded before the Petri dish was rinsed with 10 mL of the measuring solution of the next spermidine concentration to be measured. Measuring volumes of 3 mL ensured pH stability during the measurement time. Before each measurement, the system was allowed to equilibrate for 30 min.

**Borosilicate Beads.** The borosilicate beads (Cat. no. 07666, Polysciences Inc., Eppelheim, Germany) were checked for clean surfaces by scanning electron microscopy (Figure 2). Energy-

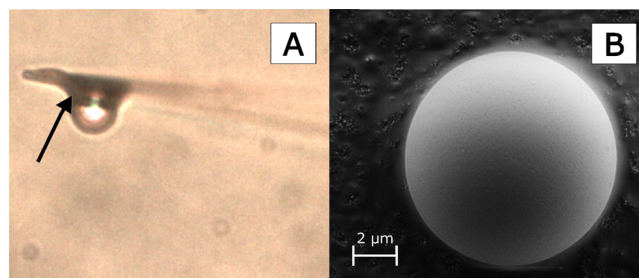


**Figure 2.** (A) Borosilicate bead glued to a cantilever behind the tip (arrow). (B) Scanning electron microscopy image of a clean bead surface.

dispersive X-ray spectroscopy tests revealed no relevant contaminations of the bead surfaces except for traces of calcium and of the omnipresent carbon atoms (data not shown). Because exact surface charge data were not available for the borosilicate beads used, we conducted measurements using single particle electrophoresis (Supporting Information). The obtained charge densities between  $-0.0115$  and  $-0.0294$  As/cm<sup>2</sup> suggest zeta potentials in the range of  $-80$  to  $-150$  mV for the measurement conditions used in the force experiments.

**Bead-Functionalized Cantilever.** For measurements, tipped (tip length: 3.5 μm), 100 μm-long, arrow-shaped, silicon-nitride cantilevers (Pyrex nitride probes, PNP-DB, NanoWorld, Neuchâtel, Switzerland) with a nominal spring constant of 0.48 N/m and a nominal resonance frequency of 67 kHz were used. The cantilevers were functionalized with the borosilicate beads, which were attached to the cantilever tips with resin glue (Endfest 300, UHU GmbH & Co KG, Bühl, Germany). To circumvent normalization of the maximum detachment forces (MDFs) and the maximum snap-to-contact force (MSFs) to the bead diameter using criteria that would depend on the mechanism of bead–surface interactions, beads with similar diameters (pH 7: 11.12 μm; pH 7.9: 10 μm; pH 9: 10.2 μm; pH 10.5: 9.9 μm; and pH 12: 8.71 μm) were microscopically selected. The functionalized cantilevers were allowed to settle for at least one day before the bonding seams between the cantilevers and beads were checked by light microscopy (Figure 2). Cantilevers with excess glue were not used. The spring constant of each cantilever was determined with the thermal noise method using a correction factor of 0.251 (second mode).<sup>30</sup> Below pH 7, the resin was destabilized, resulting in the detachment of the bead,

which prevented more elaborate measurements in the lower pH range (compare to ref 23).

**Mica Surfaces.** Muscovite mica sheets (PLANO, Wetzlar, Germany) were cut with a sharp blade to fit into the Petri dishes before being cleaved to a thickness of approx. 0.28 mm and attached to the bottom of the dishes by moderate pressure. Mica is well-known to have a negative surface charge with typical surface potentials in the range of  $-60$  to  $-130$  mV depending on the exact chemical composition of the mica type.<sup>31</sup> The negative zeta potential of mica is strongly pH-dependent in the range of pH 5 to 7 but largely constant over the pH range used in this study.<sup>25</sup>

**Registration of Force–Distance Curves.** The AFM measurements started from a force-free position. During the approach of the cantilever at a velocity of  $20 \mu\text{m/s}$ , it experienced a hydrodynamic force until bead–mica contact. Further extension led to increasing cantilever deflection, represented by a steep slope in the force–distance curve. After the setpoint force of  $1.5$  nN was reached, the cantilever was retracted at  $20 \mu\text{m/s}$ . Attractive interactions during retraction led to a downward deflection of the cantilever tip. The MDF was determined before bead detachment. The hydrodynamic force during retraction induced a deflection opposite to that during the approach. No differences in the force behavior were registered when approach and retraction velocities of  $5 \mu\text{m/s}$  were used. For further details, see refs 32 and 33.

Under certain conditions, electrostatic attraction did overcome the spring constant of the cantilever in the approach mode, resulting in a snap to contact. Snap-to-contact events are characterized by their bead-to-surface distance and the MSF. In rare cases, attraction was observed in the retraction curves up to  $800$  nm. This was attributed to debris in the measurement medium. Such exceptionally long distances were not observed at the highest spermidine concentrations used.

**Preparation of Giant Unilamellar Vesicles.** GUVs were prepared by electroformation at room temperature according to Angelova et al. with the modifications described by Tomšič et al.<sup>34,35</sup> The synthetic lipids cardiolipin (1,1',2,2'-tetraoleoylcardiolipin), POPC (1-palmitoyl-2-oleoyl-*sn*-glycero-3-phosphocholine), and cholesterol were purchased from Avanti Polar Lipids, Inc. (Alabaster, USA). Weighted amounts of POPC, cardiolipin, and cholesterol were dissolved in 2:1 chloroform/methanol (v/v) before thorough mixing. To obtain charged GUVs, cardiolipin, POPC, and cholesterol were mixed in a 4:4:2 ratio. For microscopic observations, the GUVs were transferred to the measurement chamber before agglutination was induced by spermidine addition.

**Data Interpretation.** The Young's modulus of borosilicate glass ranges from  $65$  to  $70$  GPa, whereas muscovite mica is a highly anisotropic crystal with orientation-dependent elastic constants. Its effective elastic modulus is between  $20$  and  $60$  GPa.<sup>36</sup> These values suggest that the Hertz deformation can be neglected in the investigated force range up to  $1.5$  nN. Because the surface of mica is molecularly smooth,<sup>37</sup> it must be expected that the surface roughness of the bead will determine the true contact area, which differs from the apparent contact area. For rough elastic surfaces, the true contact surface is generally proportional to the normal force, whereas the size of the microcontacts is known to only weakly depend on the load.<sup>38,39</sup>

For the beads' surface charges, Gaussian distributions were obtained (Supporting Information). This permitted ANOVA testing of the pH dependence of the surface charge. The force spectroscopy data were statistically evaluated with JMP 10 data analysis software (JMP, Böblingen, Germany) and tested for their Gaussian distribution using the Shapiro–Wilk test. Accordingly, the mean values of the force distributions were used in the following considerations.

## RESULTS AND DISCUSSION

**Force Spectra: pH and Spermidine Effects.** Figure 3 shows three different force–distance curves illustrating qualitative pH-related spermidine effects. Without spermidine, snap-to-contact and attractive forces were observed only at pH 7.0 (Figure 3A). The MSF and MDF were  $11 \pm 41$  and  $1078 \pm 951$  pN, respectively. At a slower retraction velocity ( $5 \mu\text{m/s}$ ),

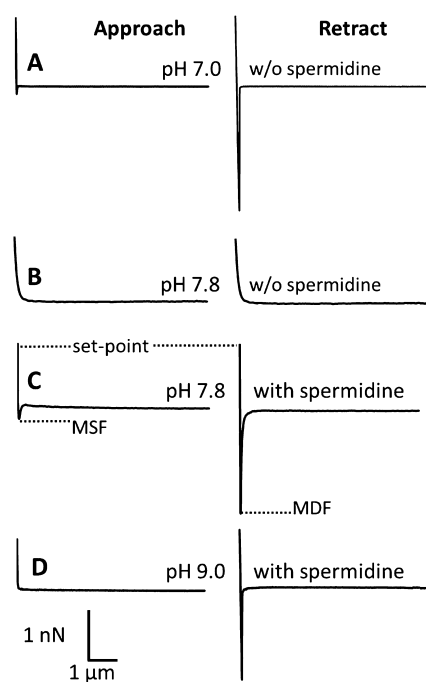


**Figure 3.** Force–distance curves measured with borosilicate beads over a mica surface. Approach (left column) and retraction (right column) curves measured at  $20 \mu\text{m/s}$ . In the absence of spermidine, MSF and MDF were detectable at pH 7.0 but not at pH 7.8 (compare curves A and B). At pH 7.0, the addition of spermidine did not significantly alter the curves. At pH 7.8, the addition of  $0.01$  mg/mL spermidine induced attraction (compare curves B and C). At this spermidine concentration, the MSF and MDF were similar to those in A (compare curves A and C). MSF disappears at pH 9.0 for spermidine concentrations of  $0.03$  mg/mL (D) and above. All data were baseline corrected. The sample rate was  $2048$  Hz.

the MDF and its standard deviation were lower than those at  $20 \mu\text{m/s}$ . An influence of the approach velocities on the MSF was not detected. In the pH ranging from 7.8 to 12, only repulsive forces were observed in both the approach and retraction profiles (Figure 3B). The detectable MDF values were below the noise level ( $1.8$  pN RMS). The addition of spermidine induced attractive interactions over the pH range of 7.8 to 10.5 but not at pH 7.0 (Figure 5). In the presence of spermidine ( $0.02$  mg/mL), the MDF decreased for increasing pH, with  $1815 \pm 275$ ,  $801 \pm 99$ , and  $25 \pm 3$  pN at pH 7.8, 9.0, and 10.5, respectively. Above pH 10.5, all attractive interactions disappeared in both the presence and absence of spermidine.

At  $20 \mu\text{m/s}$ , the largest interaction distances at which deflections of the cantilever were detectable were approx.  $100$  nm in the approach and retraction force curves in the absence of spermidine and in the presence of low and intermediate spermidine concentrations. For spermidine concentrations of  $0.1$  mg/mL and above (data not shown), snap to contact was never observed in the approach curves.

For interaction distances above  $100$  nm, electrostatic explanations can be excluded because the Debye–Hückel length was below  $100$  nm even at the very low ionic strengths used in the experiments. A possible explanation involves the soft elastic soak layers on the surfaces. Such soak layers of  $80$ – $90$  nm thickness have been described to develop on borosilicate glass but not on mica surfaces.<sup>40</sup> The layers generate complex, pH-dependent force effects, which lead to deformations in the approach curves. Here, we attribute the distortions in the

force–distance curves, which were observed especially at longer measurement times, to the indentation and elastic relaxation effects of the soak layers.

The pH dependence of the attractive interactions was most pronounced at a spermidine concentration of 0.02 mg/mL. The attraction was maximal at pH 7.8. In the presence of spermidine, the snap-to-contact distances in the approach profiles decreased with increasing pH.

Snap to contact was never observed at pH 10.5. At pH 7.8 and 9.0, the detected MSFs were  $201 \pm 32$  and  $56 \pm 5$  pN, respectively. At pH 9, the snap-to-contact disappeared at spermidine concentrations higher than 0.02 mg/mL, and repulsive interactions were detected in the approach profiles (Figure 3D). At the highest spermidine concentration of 0.1 mg/mL, repulsion was detected in all approach profiles above pH 7.8. Interestingly, attraction was detected in the retraction profiles at pH 7.8. Figure 4 summarizes the measured MDF profiles at different pH values and spermidine concentrations.

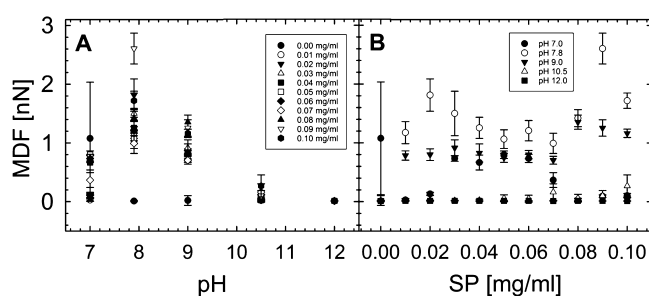


**Figure 4.** Dependence of the MDF on the pH (A) and spermidine concentration (B). For details of the error bars in (A), kindly refer to (B). MDF normalization to the bead diameter could be avoided by selecting beads with roughly identical diameters for pH 7.9 (10  $\mu$ m), pH 9 (10.2  $\mu$ m), and pH 10.5 (9.9  $\mu$ m), which determine the fitting parameters in Figures 8 and 9.

**Spermidine-Induced Attractive Interaction Between GUVs.** GUVs are spherical membrane bodies. Their physical properties, such as surface charge and membrane fluidity, are determined by their lipid composition. We produced GUVs composed of cardiolipin, POPC, and cholesterol with a negative surface charge density similar to that of biological cells, as described by Perutková et al.,<sup>41</sup> to demonstrate the biological relevance of the spermidine-induced force effects. Under physiological conditions, the GUVs were microscopically observed as well-separated spherical objects (Figure 5A). Spontaneous agglutination was observed after the addition of spermidine (Figure 5B).

**Basic Assumptions.** It is known that the surface potentials of mica and borosilicate surfaces may approach 0 mV under strongly acidic conditions.<sup>23,26</sup> Nevertheless, at pH 7.8 and above constant negative potentials with similar surface charge densities can be assumed for both like-charged surfaces, whereas the spermidine charge decreases within the measured pH range. The spermidine molecule is triprotonated at pH 7 and monoprotonated at pH 10.5.<sup>2</sup>

For simplicity, ionic strength effects were not taken into account. Because the presence of counterions other than spermidine was neglected, the spermidine concentration had to be assumed according to the electroneutrality condition, that is, higher spermidine concentrations were assumed for smaller gaps. In the simulations, a room temperature of 300 K was assumed.

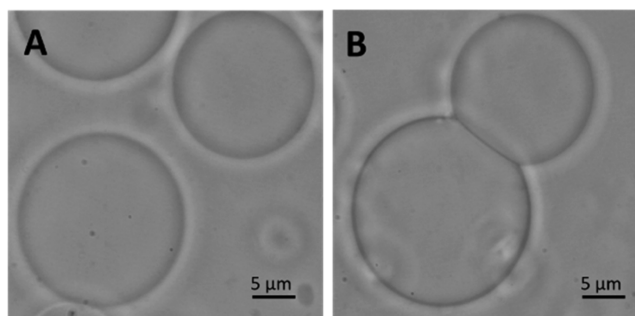


**Figure 5.** GUVs with a negative surface charge in the absence (A) and in the presence (B) of spermidine.

**Attractive Interactions without Spermidine.** For spermidine-free solutions, snap to contact at pH 7.0 can be explained by a positively charged mica surface (Figure 3A). Electrostatic repulsion would be the straightforward explanation for the observed forces at pH 7.8 (Figure 3B). Nevertheless, the correct explanation must include osmotic effects. Without ions, the aqueous gap between the like-charged surfaces would be field free. For simplicity, let us assume that only counterions are introduced into the gap to ensure electroneutrality of the whole system. The ions would repel one another and would be collected at the surface of the aqueous medium, similar to the electronic charges at the surface of a charged metallic body. The approach of the two surfaces would increase the counterion concentration inside the gap. The resulting increase in osmotic pressure would drive water into the gap, generating repulsion.<sup>31</sup> This repulsion will be higher for narrower gaps and higher counterion concentrations.<sup>42</sup> These relationships are described by the contact value theorem,<sup>17</sup> which allows the determination of the osmotic pressure from the electric properties of the system. The theorem can be applied as long as no counterions are adsorbed on the surfaces, which would change the effective surface charge densities.

**Monte-Carlo Simulations of the Orientational Ordering of Spermidine.** Monte-Carlo simulations were conducted to consider the role of the orientational ordering of the positively charged, rod-like spermidine molecules in attracting the negatively like-charged borosilicate and mica surfaces. The standard Monte Carlo Metropolis algorithm<sup>43</sup> was applied to an electroneutral, periodic system with 2D symmetry using an implementation of the Lekner–Sperb method.<sup>44,45</sup> The algorithm used was similar to that of Moreira and Netz.<sup>46</sup> The canonical system of 100 diprotonated molecules considered was constrained by two impenetrable charged surfaces, which were treated as planar with respect to the size of the molecules. For simplicity, the simulations were only performed for diprotonated molecules. In each simulation step, a single molecule was randomly chosen and randomly translated or rotated around its center, assuming the same probability for the two types of movement. The run time of a simulation was approx.  $5 \times 10^7$  steps. For the protonation sites, pointlike charges with two different separation distances of  $L = 1$  nm (rodlike model) and  $L = 0.01$  nm (pointlike model) were considered (see Figures 6 and 7). The assumption of pointlike diprotonated molecules with  $L = 0.01$  nm permitted the comparison of the Monte-Carlo results with the predictions of the Poisson–Boltzmann standard model.

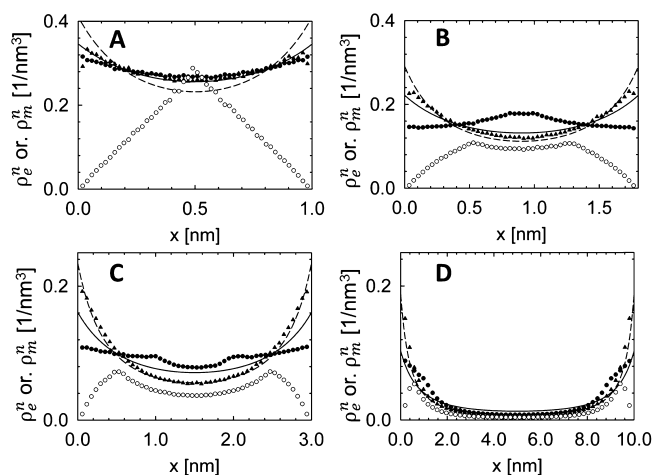


**Figure 6.** Spatial distributions of the number densities of the centers of mass (open circles) and of the elementary charges (filled symbols) for diprotonated rodlike and pointlike molecules at surface charge densities of  $0.023 \text{ A s/m}^2$  and gap widths of 1 (A), 1.8 (B), 3 (C), and 10 nm (D). The distributions were obtained by Monte-Carlo simulations with intramolecular charge separation distances of  $L = 1 \text{ nm}$  (filled circles) and  $L = 0.01 \text{ nm}$  (filled triangles). The results of the mean-field Poisson–Boltzmann theory for monovalent (solid line) and diprotonated (dashed line) molecules are given for comparison.

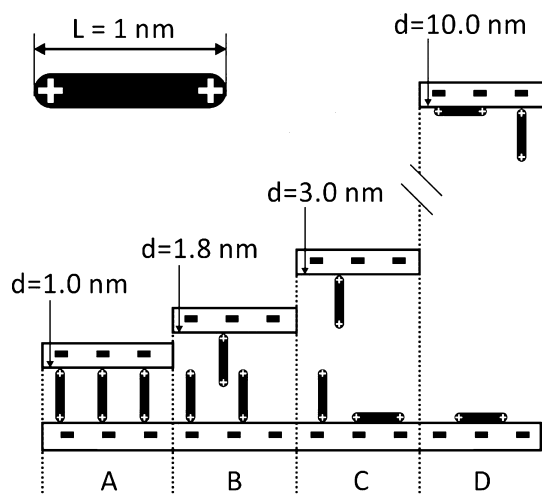


**Figure 7.** Schematic representation of oriented diprotonated rodlike molecules of length  $L$  in gaps of width  $d$ . Perpendicularly oriented molecules mediate the attractive short-range bridging forces between the negatively like-charged surfaces (A). Panels C and D show perpendicularly and parallelly oriented molecules.

Figure 6 presents the spatial distributions of the number densities of the molecular centers of mass and of the elementary charges for gap widths of 1, 1.8, 3, and 10 nm. For comparison, the results of the Poisson–Boltzmann model are presented for monoprotonated and diprotonated pointlike molecules.

For a gap width of  $d = 1 \text{ nm}$ , the number density of the centers of mass shows a maximum at  $x = d/2$ , that is, at the midplane between the two surfaces (Figure 6A). This gap width corresponds to the length  $L = 1 \text{ nm}$  of the rodlike model. The roof shape of the density distribution results from the increasing steric restrictions in the spherical gyration of molecules, which approach the hard wall surfaces. For  $d = 1 \text{ nm}$ , free rotation is ensured only for positions of the molecular

centers at  $x = d/2$ . For larger gap widths, two peaks are obtained in the number density of the centers of mass, appearing approximately  $0.5 L$  away from the surfaces (Figure 6B–D). For gap widths of  $d = 10 \text{ nm} \gg L$  (Figure 6D), a relatively high number of molecules are attached in parallel to the surfaces, resulting in increased number densities of the centers of mass and of the charges near the surfaces. At this gap width, the charge distribution profiles of the Monte-Carlo simulations and of the Poisson–Boltzmann mean-field approach almost overlap for diprotonated pointlike molecules. This hints at the convergence of the two approaches for larger gap widths and small  $L$  values. At a very short distance from the surfaces, the Monte-Carlo profiles are decreased because of entropic effects driven by the thermal motion of the molecules.

For the rodlike model, the degree of rotational freedom is reflected in the contribution of the rotational entropy to the total free energy of the system. Accordingly, the predicted peak positions in the number density distributions of the centers of mass correspond to optimal positions for a minimal free energy of the system. For a gap width of  $d \approx L$ , the highest number density of the centers of mass was predicted at the midplane, whereas the number density of elementary charges was lowest at this position (Figure 6A). Molecules located with their centers of mass at the midplane, may electrostatically interact with both charged surfaces. For larger gap widths, electrostatic interaction must occur predominantly with either one of the charged surfaces (Figures 6B–D and 7).

For  $d = 1.8 \text{ nm}$ , the mass number density profile shows minute peaks at surface distances of approximately  $L/2$ . The corresponding charge number density profile exhibits two weak maxima around a distance  $L$  from both charged surfaces, suggesting that a considerable number of molecules is attached in a perpendicular orientation. The free ends of these molecules overlap in the midplane (Figure 7B), generating a charge number density that is larger than those near the surfaces (Figure 6B). When the two surfaces are approaching in the presence of diprotonated rodlike molecules, the local increase in the charge number density at the midplane creates a local electrostatic energy barrier,<sup>13</sup> which must be overcome during the approach or retraction of the surfaces. It can be assumed that the electrostatic repulsion of the charged molecular tips generates forces, which induce correlated charge patterns when the tip layers penetrate one another.

These properties result in strong deviations of the charge number densities predicted by the Poisson–Boltzmann theory for pointlike charges, especially for gap widths of 1.8 and 3.0 nm (Figure 6B,C).

At a gap width of 3.0 nm, the charge number density profile shows small peaks at a distance of 1 nm from the surfaces. This is the distance bridged by molecules that are perpendicularly attached to the surfaces (Figure 6C). Because of the increasing number of molecules with nonperpendicular orientations, the charge number density at the surfaces slightly exceeds the 1 nm peaks.

Figure 7 presents the positions and orientations of rodlike molecules within the gap. The figure illustrates the special features found in the Monte-Carlo simulation, such as intermolecular charge correlation and steric restrictions in the spatial distributions of mass centers and charges. For clarity in the schematic presentation, the majority of molecules are neglected. The total number of molecules in the simulations was determined from the electroneutrality condition in the gap, which is schematically fulfilled in Figure 7. Molecules attached

to the surfaces in parallel orientation reduce the effective surface charge densities at larger gap widths.

The order parameters  $S$  given in Table 1 were averaged over the degree of orientational ordering of the diprotonated

**Table 1. Averaged Order Parameters  $S$  of Diprotonated Rodlike Molecules between Two Like-Charged Surfaces for Different Gap Widths ( $d$ )**

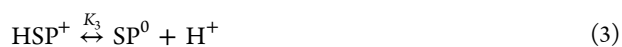
$d$ [nm]	$S$
1.0	-0.235
1.8	-0.091
3.0	-0.073
10.0	-0.067

spermidine molecules for the gap widths in Figure 7.<sup>41</sup> As described therein, the random orientation of the rodlike molecules corresponds to  $S = 0$ , whereas the average orientations in parallel and perpendicular to the charged surfaces correspond to  $S = -0.5$  and  $S = 1$ , respectively.

The order parameter for  $d = 1$  nm indicates that only a minority of molecules are oriented perpendicular to the surfaces. At first glance, this is due to steric effects because only molecules with a center of mass located at the midplane may orient perpendicular to the surfaces (see also Figure 6A). The closer the center of mass is to one of the surfaces, the stronger the steric restrictions are, resulting in a more parallel orientation to the surface. Actually, the orientation is predominantly because of electrostatic effects. Namely, for a gap width of 1 nm and large surface charge densities, a considerable number of molecules are located with their center of mass in the vicinity of the midplane, generating strong attractive bridging forces between the like-charged surfaces (Figure 6A). For larger gap widths, the order parameter approaches zero because the two charges of the rodlike molecules cannot interact with both planar surfaces at the same time.

**pH-Dependent Spermidine Charge and MDF: a Phenomenological Model.** The decrease in MDF with increasing pH (Figure 4) suggests that the triprotonated spermidine species make the highest contributions to the MDF. The contribution decreases for diprotonated, monoprotated, and nonprotonated spermidine.

The pH-dependent probability of the protonation of the three N groups depends on their position within the spermidine molecule. This probability is described by the  $pK_a$  values of 8.25, 9.71, and 10.90, permitting the titration to determine the molecule's overall charge number. Over our experimental pH range, the protonation is changed from 1+ to 2+ at approximately pH 10.5 and from 2+ to 3+ at approximately pH 8.5. The protonation of spermidine is described by three equilibrium reactions with the equilibrium constants  $K_1$ ,  $K_2$ , and  $K_3$



The equilibrium constants  $K_1$ ,  $K_2$ , and  $K_3$  were derived by Kimberly and Goldstein from the chemical shifts observed in <sup>13</sup>C NMR experiments.<sup>2</sup> The overall spermidine concentration

[SP] is the sum of the non- [SP<sup>0</sup>], mono- [HSP<sup>+</sup>], di- [H<sub>2</sub>SP<sup>2+</sup>], and triprotonated [H<sub>3</sub>SP<sup>3+</sup>] spermidine species

$$[\text{SP}] = [\text{SP}^0] + [\text{H}_2\text{SP}^{2+}] + [\text{H}_2\text{SP}^{2+}] + [\text{H}_3\text{SP}^{3+}] \quad (4)$$

Correlating the abundance of the different spermidine species to the generated MDF, the MDF is

$$\text{MDF} = f_0[\text{SP}^0] + f_1[\text{HSP}^+] + f_2[\text{H}_2\text{SP}^{2+}] + f_3[\text{H}_3\text{SP}^{3+}] \quad (5)$$

with the constants  $f_0$ ,  $f_1$ ,  $f_2$ , and  $f_3$  weighting the specific MDF contributions of each species. To reduce the number of free parameters in the pH-dependent MDF equation, the weak force contributions of the nonprotonated and monoprotated spermidine species were neglected ( $f_0 = f_1 = 0$ ). The concentrations of the triprotonated [H<sub>3</sub>SP<sup>3+</sup>] and diprotonated species [H<sub>2</sub>SP<sup>2+</sup>] are

$$[\text{H}_3\text{SP}^{3+}] = \frac{[\text{H}^+]^3[\text{SP}]}{[\text{H}^+]^3 + [\text{H}^+]^2K_1 + [\text{H}^+]K_1K_2 + K_1K_2K_3} \quad (6)$$

$$[\text{H}_2\text{SP}^{2+}] = \frac{K_1[\text{H}^+]^2[\text{SP}]}{[\text{H}^+]^3 + [\text{H}^+]^2K_1 + [\text{H}^+]K_1K_2 + K_1K_2K_3} \quad (7)$$

The pH-dependent MDF is described by the sigmoidal decay function

$$\text{MDF} = \frac{[\text{H}^+]^2[\text{SP}](f_3 + f_2K_1)}{[\text{H}^+]^3 + [\text{H}^+]^2K_1 + [\text{H}^+]K_1K_2 + K_1K_2K_3} \quad (8)$$

The force constants  $f_2$  and  $f_3$  were obtained by fitting the MDF to the pH values and spermidine concentrations.

In contrast to Figure 4, Figure 8 shows individual fits to the MDF data at certain spermidine concentrations. The plateau of

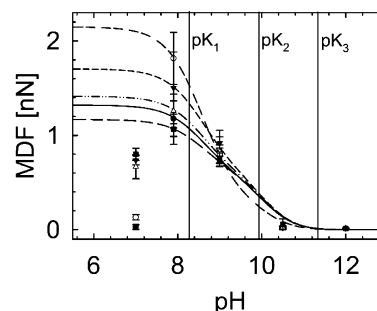


**Figure 8.** MDF dependence on pH. The curves are fits of eq 8 ( $R^2 = 0.95$ ) to the data in Figure 4 (0.01 mg/mL (filled circles/solid line), 0.02 mg/mL (open circles/medium-dashed line), 0.03 mg/mL (filled triangles pointed down/short-dashed line), 0.04 mg/mL (open triangles/dash-dotted line) and 0.05 mg/mL (filled squares/long-dashed line)). The measurement points at pH 7 were excluded from the fit.

these pH-dependent curves is defined by  $f_3$ , that is, the maximum contribution of the triprotonated spermidine. At the first glance, the most striking difference from that in Figure 4 is the inconstant plateau height at different spermidine concentrations. However, as one can see from Figure 8, there is no obvious trend in differing plateau heights for increasing spermidine concentrations. In addition to the strong variation in the plateau height, a change in the position of the decay flank near  $pK_1$  is also observed.

In Figure 9, the measured points of each spermidine concentration were fitted using eq 8. Systematic features are

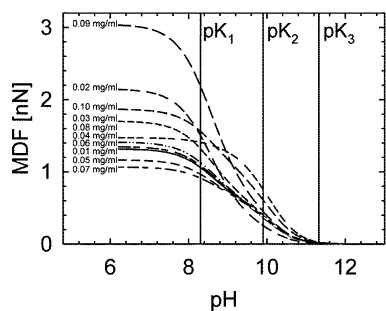


**Figure 9.** Sigmoidal fit of the MDFs (eq 7) for the dependence on the spermidine concentration.

difficult to comprehend from the plot. Nevertheless, Figure 10 reveals a characteristic spermidine concentration dependence of  $f_2$  and  $f_3$ .

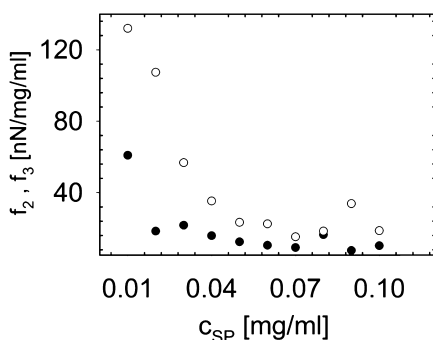


**Figure 10.** Calculated force coefficients  $f_2$  and  $f_3$  of the diprotonated (open circles) and triprotonated (filled circles) spermidine species at different spermidine concentrations (see eqs 5 and 8).

The decreasing force contributions toward higher spermidine concentrations suggest that the surfaces are saturated above 0.05 mg/mL. This is in line with an MSF that disappeared above 0.02 mg/mL and turned into repulsion at pH 9.0 (Figure 3D).

## CONCLUSIONS

Our experiments showed that spermidine may induce electrostatic attraction between the negatively like-charged surfaces of borosilicate and mica. One possibility to explain this finding is to employ the DLVO theory. It describes the total interaction energy between objects or surfaces by superimposed exponential functions with specific distance dependencies.<sup>47</sup> In the theory, the electrostatic repulsion between two like-charged surfaces may be overcome by attractive van der Waals forces. At short distances, also small counterions may induce electrostatic attraction.<sup>20</sup> In addition to its electrostatic effect, for spermidine, stronger van der Waals attractions can be expected for spermidine than for smaller inorganic ions.

Our Monte-Carlo simulations of the orientational ordering showed that a certain percentage of the rodlike spermidine molecules is attached to the surfaces in perpendicular orientation. At small gap widths, polyvalent spermidine molecules mediate the “bridging force mechanism”, an electrostatic bridge-pull effect between the like-charged surfaces.<sup>14,41,48</sup> At higher surface charges, the mechanism is

more effective because the amount of perpendicularly oriented molecules is increased. The simulations also predicted a considerable number of spermidine molecules that are condensed on the surfaces in a parallel orientation. These molecules diminish the effective surface charge densities and reduce the electrostatic repulsion of the surfaces for larger gaps.<sup>41</sup> For narrow gaps, the lower effective surface charge densities reduce the counterion concentration and in turn the osmotic surface repulsion.

It is generally accepted that attractions between similarly charged objects cannot be explained using the Poisson–Boltzmann mean-field approach, assuming pointlike charges. However, in biological molecules, such as spermidine, the charges are located at distinct distances. Orientational ordering and “intraionic” positional correlations are described for molecular models with pointlike charges of finite separation distances. The effects induce short-range attraction (bridging effects) between similarly charged objects, which can be predicted using a refined mean-field approach.<sup>10,14,41,48</sup> Short-range attractions induced by bridging effects have been confirmed by Monte-Carlo simulations.<sup>14</sup>

In the experiments, repulsion (no MSF) was detected above 0.02 mg/mL spermidine at pH 9.0, where the molecules were mostly diprotonated (Figure 3D). A possible explanation involves the reduced effective surface charge by the molecules attached to the surface in parallel orientation (Figure 7D) and an energy barrier generated by the repulsion of the positively charged headgroups of the perpendicularly oriented spermidine molecules approaching the midplane (cf. to discussion on ion correlation in the text). When the setpoint force overcomes this barrier, the “bridging force mechanism” may come into effect, inducing the detected MDF. In contrast, no repulsion was observed at pH 7.8, independent of spermidine concentration. We suggest that the higher effective charge of the di- and triprotonated spermidine species at this pH reduces the effective surface charge, leading to reduced free energy of the surfaces and decreased electrostatic repulsion (Figure 3C, compare to  $f_2$ ,  $f_3$  in Figure 10). Large polyions may even overcompensate for the surface charge, inducing a charge reversal of one or both surfaces, which may explain the lack of repulsion or a more complex behavior.<sup>49</sup> We believe that our model system provides a platform for studying the mechanism behind the force interactions between like-charged surfaces. AFM measurement with GUVs will be complicated. For liposomes with diameters larger than 150 nm, there is a delicate balance between the adhesion of stable spherical structures and spreading.<sup>50</sup>

## ASSOCIATED CONTENT

### Supporting Information

The Supporting Information is available free of charge on the ACS Publications website at DOI: 10.1021/acs.langmuir.7b04199.

Surface charge of the borosilicate beads determined by particle electrophoresis (PDF)

## AUTHOR INFORMATION

### Corresponding Authors

\*E-mail: jan.gimsa@uni-rostock.de. Phone: +49 381 498 6020.

Fax: +49 381 498 6022 (J.G.).

\*E-mail: ales.iglic@fe.uni-lj.si (A.I.).

ORCID 

Jan Gimsa: 0000-0003-1495-9434

## Author Contributions

J.G., P.W., and Š.P. contributed equally. The manuscript was written through contributions of all authors. All authors have given approval to the final version of the manuscript.

## Funding

European Fund for Regional Development (V220-630-08-TFMV-F-011), European Social Fund (V220-630-08-TFMV-F-011), and National Science Foundation, USA (MCB-1052208), German Research Council (GRK1505/2).

## Notes

The authors declare no competing financial interest.

## ACKNOWLEDGMENTS

The authors are grateful to the DFG (German Research Council) graduate school GRK1505/2 “Welisa” for funding the PhD positions of P.W. and T.W. and consumables for the experiments. We are grateful to Mojca Frank-Bertoncelj, University Hospital Zürich, Switzerland, for providing the liposome pictures. Dr. Andreas Körtge, University of Rostock, Germany, is acknowledged for his help in the AFM experiments.

## ABBREVIATIONS

AFM, atomic-force microscopy; GUV, giant unilamellar vesicle; MDF, maximum detachment force; MSF, maximum snap-to-contact force; POPC, 1-palmitoyl-2-oleoyl-*sn*-glycero-3-phosphocholine

## REFERENCES

- (1) Khan, A. U.; Mei, Y. H.; Wilson, T. A proposed function for spermine and spermidine: protection of replicating DNA against damage by singlet oxygen. *Proc. Natl. Acad. Sci. U.S.A.* **1992**, *89*, 11426–11427.
- (2) Kimberly, M. M.; Goldstein, J. H. Determination of pKa values and total proton distribution pattern of spermidine by carbon-13 nuclear magnetic resonance titrations. *Anal. Chem.* **1981**, *53*, 789–793.
- (3) Minois, N. Molecular basis of the ‘anti-aging’ effect of spermidine and other natural polyamines—a mini-review. *Gerontology* **2014**, *60*, 319–326.
- (4) Cohn, M. S.; Tabor, C. W.; Tabor, H.; Wickner, R. B. Spermidine or spermine requirement for killer double-stranded RNA plasmid replication in yeast. *J. Biol. Chem.* **1978**, *253*, 5225–5227.
- (5) Eisenberg, T.; Knauer, H.; Schauer, A.; Büttner, S.; Ruckenstein, C.; Carmona-Gutierrez, D.; Ring, J.; Schroeder, S.; Magnes, C.; Antonacci, L.; Fussi, H.; Deszcz, L.; Hartl, R.; Schraml, E.; Criollo, A.; Megalou, E.; Weiskopf, D.; Laun, P.; Heeren, G.; Breitenbach, M.; Grubeck-Loebenstien, B.; Herker, E.; Fahrenkrog, B.; Fröhlich, K.-U.; Sinner, F.; Tavernarakis, N.; Minois, N.; Kroemer, G.; Madeo, F. Induction of autophagy by spermidine promotes longevity. *Nat. Cell Biol.* **2009**, *11*, 1305–1314.
- (6) Frank, M.; Manček-Keber, M.; Kržan, M.; Sodin-Šemrl, S.; Jerala, R.; Igljč, A.; Rozman, B.; Kralj-Igljč, V. Prevention of microvesiculation by adhesion of buds to the mother cell membrane—a possible anticoagulant effect of healthy donor plasma. *Autoimmun. Rev.* **2008**, *7*, 240–245.
- (7) Liquori, A. M.; Costantino, L.; Crescenzi, V.; Elia, V.; Giglio, E.; Puliti, R.; De Santis Savino, M.; Vitagliano, V. Complexes between DNA and polyamines: a molecular model. *J. Mol. Biol.* **1967**, *24*, 113–122.
- (8) Raspaud, E.; Durand, D.; Livolant, F. Interhelical spacing in liquid crystalline spermine and spermidine-DNA precipitates. *Biophys. J.* **2005**, *88*, 392–403.
- (9) Chatteraj, D. K.; Gosule, L. C.; Schellman, J. A. DNA condensation with polyamines. *J. Mol. Biol.* **1978**, *121*, 327–337.
- (10) Bohinc, K.; Igljč, A.; May, S. Interaction between macroions mediated by divalent rod-like ions. *Europhys. Lett.* **2004**, *68*, 494–500.
- (11) Hallab, N. J.; Bundy, K. J.; O’Connor, K.; Clark, R.; Moses, R. L. Cell adhesion to biomaterials: correlations between surface charge, surface roughness, adsorbed protein, and cell morphology. *J. Long-Term Eff. Med. Implants* **1995**, *5*, 209–231.
- (12) Stevens, M. M.; George, J. H. Exploring and engineering the cell surface interface. *Science* **2005**, *310*, 1135–1138.
- (13) Lokar, M.; Urbanija, J.; Frank, M.; Hägerstrand, H.; Rozman, B.; Bobrowska-Hägerstrand, M.; Igljč, A.; Kralj-Igljč, V. Agglutination of like-charged red blood cells induced by binding of beta2-glycoprotein I to outer cell surface. *Bioelectrochemistry* **2008**, *73*, 110–116.
- (14) Urbanija, J.; Bohinc, K.; Bellen, A.; Maset, S.; Igljč, A.; Kralj-Igljč, V.; Kumar, P. B. S. Attraction between negatively charged surfaces mediated by spherical counterions with quadrupolar charge distribution. *J. Chem. Phys.* **2008**, *129*, 105101.
- (15) Gongadze, E.; Kabaso, D.; Bauer, S.; Slivnik, T.; Schmuki, P.; van Rienen, U.; Igljč, A. Adhesion of osteoblasts to a nanorough titanium implant surface. *Int. J. Nanomed.* **2011**, *6*, 1801–1816.
- (16) Cowley, A. C.; Fuller, N. L.; Rand, R. P.; Parsegian, V. A. Measurement of repulsive forces between charged phospholipid bilayers. *Biochemistry* **1978**, *17*, 3163–3168.
- (17) Israelachvili, J. N. *Intermolecular and Surface Forces: Revised Third Edition*, 3rd ed.; Elsevier Science: Burlington, 2011.
- (18) Wozniak, M. A.; Modzelewska, K.; Kwong, L.; Keely, P. J. Focal adhesion regulation of cell behavior. *Biochim. Biophys. Acta* **2004**, *1692*, 103–119.
- (19) Guldbrand, L.; Jönsson, B.; Wennerström, H.; Linse, P. Electrical double layer forces. A Monte Carlo study. *J. Chem. Phys.* **1984**, *80*, 2221–2228.
- (20) Kjellander, R.; Marcelja, S.; Pashley, R. M.; Quirk, J. P. Double-layer ion correlation forces restrict calcium-clay swelling. *J. Phys. Chem.* **1988**, *92*, 6489–6492.
- (21) Wennerström, H.; Jönsson, B.; Linse, P. The cell model for polyelectrolyte systems. Exact statistical mechanical relations, Monte Carlo simulations, and the Poisson–Boltzmann approximation. *J. Chem. Phys.* **1982**, *76*, 4665–4670.
- (22) Oosawa, F. Counterion fluctuation and dielectric dispersion in linear polyelectrolytes. *Biopolymers* **1970**, *9*, 677–688.
- (23) Hartley, P. G.; Larson, I.; Scales, P. J. Electrokinetic and Direct Force Measurements between Silica and Mica Surfaces in Dilute Electrolyte Solutions. *Langmuir* **1997**, *13*, 2207–2214.
- (24) Guggenheim, S.; Yu-Hwa, C.; van Groos, A. F. K. Muscovite dehydroxylation: High-temperature studies. *Am. Mineral.* **1987**, *72*, 537–550.
- (25) Riedel, E. *Allgemeine und Anorganische Chemie: Ein Lehrbuch für Studenten mit Nebenfach Chemie*, 6th ed.; De Gruyter: Berlin, New York, 1994.
- (26) Scales, P. J.; Grieser, F.; Healy, T. W.; White, L. R.; Chan, D. Y. C. Electrokinetics of the silica-solution interface: a flat plate streaming potential study. *Langmuir* **1992**, *8*, 965–974.
- (27) Kosmulski, M. pH-dependent surface charging and points of zero charge. *J. Colloid Interface Sci.* **2006**, *298*, 730–741.
- (28) Hareme, D. L.; Bousse, L. J.; Shott, J. D.; Meindl, J. D. Ion-sensing devices with silicon nitride and borosilicate glass insulators. *IEEE Trans. Electron Devices* **1987**, *34*, 1700–1707.
- (29) James, R. O.; Parks, G. A. Characterization of Aqueous Colloids by Their Electrical Double-Layer and Intrinsic Surface Chemical Properties. *Surface and Colloid Science*; Springer, 1982; pp 119–216.
- (30) Hutter, J. L.; Bechhoefer, J. Calibration of atomic-force microscope tips. *Rev. Sci. Instrum.* **1993**, *64*, 1868–1873.
- (31) Israelachvili, J. N.; Adams, G. E. Measurement of forces between two mica surfaces in aqueous electrolyte solutions in the range 0–100 nm. *J. Chem. Soc., Faraday Trans. 1* **1978**, *74*, 975–1001.
- (32) Elter, P.; Weihe, T.; Bühler, S.; Gimsa, J.; Beck, U. Low fibronectin concentration overcompensates for reduced initial

fibroblasts adhesion to a nanoscale topography: single-cell force spectroscopy. *Colloids Surf, B* **2012**, *95*, 82–89.

(33) Elter, P.; Weihe, T.; Lange, R.; Gimsa, J.; Beck, U. The influence of topographic microstructures on the initial adhesion of L929 fibroblasts studied by single-cell force spectroscopy. *Eur. Biophys. J.* **2011**, *40*, 317–327.

(34) Angelova, M. I.; Soléau, S.; Méléard, P.; Faucon, F.; Bothorel, P. Preparation of giant vesicles by external AC electric fields. Kinetics and applications. *Prog. Colloid Polym. Sci.* **1992**, *89*, 127–131.

(35) Tomšič, N.; Babnik, B.; Lombardo, D.; Mavčič, B.; Kandušer, M.; Igljč, A.; Kralj-Igljč, V. Shape and size of giant unilamellar phospholipid vesicles containing cardiolipin. *J. Chem. Inf. Model.* **2005**, *45*, 1676–1679.

(36) McNeil, L. E.; Grimsditch, M. Elastic moduli of muscovite mica. *J. Phys.: Condens. Matter* **1993**, *5*, 1681–1690.

(37) Yu, J.; Namba, Y. Atomic surface roughness. *Appl. Phys. Lett.* **1998**, *73*, 3607–3609.

(38) Archard, J. F. Elastic Deformation and the Laws of Friction. *Proc Royal Soc A* **1957**, *243*, 190–205.

(39) Greenwood, J. A.; Williamson, J. B. P. Contact of Nominally Flat Surfaces. *Proc Royal Soc A* **1966**, *295*, 300–319.

(40) Preuss, M.; Butt, H.-J. Direct Measurement of Particle–Bubble Interactions in Aqueous Electrolyte: Dependence on Surfactant. *Langmuir* **1998**, *14*, 3164–3174.

(41) Perutková, Š.; Frank, M.; Bohinc, K.; Bobojevič, G.; Zelko, J.; Rozman, B.; Kralj-Igljč, V.; Igljč, A. Interaction between equally charged membrane surfaces mediated by positively and negatively charged macro-ions. *J. Membr. Biol.* **2010**, *236*, 43–53.

(42) Joensson, B.; Wennerstroem, H.; Halle, B. Ion distributions in lamellar liquid crystals. A comparison between results from Monte Carlo simulations and solutions of the Poisson–Boltzmann equation. *J. Phys. Chem.* **1980**, *84*, 2179–2185.

(43) Metropolis, N.; Rosenbluth, A. W.; Rosenbluth, M. N.; Teller, A. H.; Teller, E. Equation of State Calculations by Fast Computing Machines. *J. Chem. Phys.* **1953**, *21*, 1087–1092.

(44) Lekner, J. Summation of Coulomb fields in computer-simulated disordered systems. *Physica A* **1991**, *176*, 485–498.

(45) Sperb, R. An Alternative to Ewald Sums part I: Identities for Sums. *Mol. Simul.* **1998**, *20*, 179–200.

(46) Moreira, A. G.; Netz, R. R. Simulations of counterions at charged plates. *Eur. Phys. J. E: Soft Matter Biol. Phys.* **2002**, *8*, 33–58.

(47) Kjellander, R.; Greberg, H. Mechanisms behind concentration profiles illustrated by charge and concentration distributions around ions in double layers. *J. Electroanal. Chem.* **1998**, *450*, 233–251.

(48) May, S.; Igljč, A.; Reščič, J.; Maset, S.; Bohinc, K. Bridging like-charged macroions through long divalent rodlike ions. *J. Phys. Chem. B* **2008**, *112*, 1685–1692.

(49) Kjellander, R. Ion-ion correlations and effective charges in electrolyte and macroion systems. *Ber. Bunsen-Ges.* **1996**, *100*, 894–904.

(50) Jaskiewicz, K.; Makowski, M.; Kappl, M.; Landfester, K.; Kroeger, A. Mechanical properties of poly(dimethylsiloxane)-block-poly(2-methyloxazoline) polymersomes probed by atomic force microscopy. *Langmuir* **2012**, *28*, 12629–12636.